A Novel High Data Rate Prerake DS UWB Multiple Access System: Interference Modeling and Tradeoff Between Energy Capture and Imperfect Channel Estimation Effect

Wei Cao, *Student Member, IEEE*, A. Nallanathan, *Senior Member, IEEE*, and Chin Choy Chai, *Member, IEEE*

***Abstract*—A novel High Data Rate (HDR) Prerake DS UWB multiple access system is proposed, in which the number of taps in the Prerake filter is set to a large value while keeping the number of taps in a chip sufficiently small. Thus high data rate can be achieved via superposition of the chip waveforms, where the inter-chip interference introduced is small due to signal energy focusing. We derive the higher order moments of Multiple Access Interference (MAI) and fit the distribution of MAI using a generalized Gaussian distribution. Numerical results show that the generalized Gaussian distribution is a more appropriate statistical model for the distribution of MAI than the Gaussian distribution. Using the Characteristic Function (CF) method, an accurate BER formula is derived and validated by numerical results. The effect of imperfect channel estimation is discussed in detail. We highlight that under imperfect channel estimation, there is a tradeoff between the signal energy captured and the channel estimation noise introduced.**

***Index Terms*—Prerake, time reversal, ultra wideband, direct sequence, multiple access, interference modeling, bit error rate, characteristic function, imperfect channel estimation**

I. Introduction

ONE of the main advantages of UWB radio lies in its extremely wide bandwidth, which leads to fine time resolution and significantly reduces fading effects even in a dense multipath environment [1]. However, how to effectively capture signal energy in such a dense multipath environment is a challenging task. If the Rake receiver is used to combine multipath components in a typical UWB channel, a large number of taps (or Rake fingers) are generally needed to capture enough signal energy [2]. For a handset, such a design is high complexity/cost.

To simplify the receiver structure, the Prerake technique has been studied for UWB communications. Origin of the Prerake technique can be found in time-division duplex (TDD) CDMA mobile communication systems [3] [4]. Principle of the Prerake technique is that the transmitter prefilters the original signal using temporally reversed channel impulse response before transmission[1]. When the preraked transmitted signal convolves with the channel impulse response, a strong peak is produced at the output of the channel. By transferring the complex Rake processing to the transmitter side, a simple receiver with only one tap is used to capture the peak. Besides the low complexity/cost receiver structure, another notable benefit of the Prerake technique is the signal energy focusing in both space and time domains. This property not only helps to reduce inter-chip interference (ICI) and MAI, but also allows high data rate transmission in channels with large delay spread. Moreover, the temporal/spatial signal energy focusing, to some extent, provides low probability of detection and location related security in multiple access systems [5].

Recent works on Prerake UWB systems are summarized as follows. **1)** The introduction of the Prerake UWB system and its comparison with the Rake UWB system can be found in [8] [9]. Simulation results in [9] show that, in a single user scenario, Prerake and Rake UWB systems achieve almost the same BER performance when the number of taps in the Prerake filter and the number of taps in the Rake receiver are the same. **2)** The MMSE structure is proposed to be used alone or together with time reversal prefilter in UWB systems to optimally combine signal energy [6] [10]. In [6], a MMSE equalizer is combined with a time reversal prefilter to optimally combine signal energy carried by a few taps including the peak and non-peak taps. Prefilters implemented using MMSE and time reversal technique are compared in [10] for a multiple input single output UWB system, which shows that the MMSE prefilter achieves better performance at the cost of higher complexity. **3)** The implementation of Prerake filter needs the channel information, and the channel estimation issue is discussed in [5] [11]. A low-complexity time reversal prefilter is proposed in [5] using a 3-level A/D conversion to simplify the channel estimation, and system performance is examined in a single user scenario. A Prerake UWB system with channel-phase-precode is proposed in [11], which uses the channel phase instead of channel gain to reduce the channel estimation feedback workload. **4)** Various

Manuscript received March 31, 2007; revised August 13, 2007; accepted October 21, 2007. The associate editor coordinating the review of this paper and approving it for publications is Z. Tian. This work was supported by the National University of Singapore, Singapore under URC Grant R-263-000-436-123.

W. Cao and A. Nallanathan are with the Department of Electrical and Computer Engineering, National University of Singapore (e-mail: {caowei, elena}@nus.edu.sg).

C. C. Chai is with the Institute for Infocomm Research, Singapore (e-mail: chaicc@i2r.a-star.edu.sg).

Digital Object Identifier 10.1109/TWC.2008.070344.

[1]Another similar prefiltering technique, called time reversal, has also been used in UWB communications [5] [6]. Nevertheless, time reversal can be continuous-time processing based on physical waveform recording and has more applications such as underwater acoustic communications [7].

interference in Prerake UWB systems is discussed in [12] [13]. Effect of inter-pulse interference (IPI) and narrowband interference is studied in [12], and a zero-forcing equalizer is proposed to overcome IPI. In [13], performance of a Prerake DS UWB system is investigated in the presence of self interference and MAI.

Signal energy focusing in the time domain allows high data rate transmission in Prerake UWB systems. So far, the Prerake UWB system supporting high data rate transmission has not been well studied. In our previous work [13], the tradeoff between data rate and BER performance is studied for a Partial-Prerake DS UWB multiple access system under perfect channel estimation. To achieve higher data rate, the number of taps in the Prerake filter (equivalent to the number of paths combined in energy capture) is decreased. As a result, BER performance of the Partial-Prerake DS UWB system degrades quickly with the growth of data rate. In this paper, we propose a novel HDR Prerake DS UWB system, in which high data rate is achieved by superposition of chip waveforms. Though the superposed chip waveforms introduce ICI, signal energy focusing helps to keep ICI sufficiently small. Numerical results show that the HDR Prerake DS UWB system yields better BER performance than the Partial-Prerake DS UWB system in high data rate scenarios. The generalized Gaussian distribution is adopted as a more appropriate model for the distribution of MAI. Then BER formula is derived using the CF method. Accuracy of the BER formula is verified by numerical results. Furthermore, effect of imperfect channel estimation is discussed in detail.

II. System Model

A. Channel Model

According to [14], channel impulse response of the k^{th} user is modeled as

$$h^{(k)}(t) = \sum_{l=0}^{L-1} \alpha_{l,k}\delta(t - \tau_{l,k}) \tag{1}$$

where L denotes the number of multipaths, $\alpha_{l,k}$ is the log-normal path gain with random phase of ± 1 and $\tau_{l,k}$ stands for the delay of the l^{th} path. For different k and l, $\alpha_{l,k}$ are independent random variables. We consider a resolvable multipath channel [15] with $\tau_{l,k} = \tau_{0,k} + lT_p$, where T_p is the width of the UWB monocycle $z(t)$. Since multipath components arrive in clusters rather than in a continuum [14], the l^{th} path can be expressed as the j^{th} ray in the i^{th} cluster. Therefore $\tau_{l,k} = \mu_{i,k} + \nu_{j,i,k}$, where $\mu_{i,k}$ is the delay of the i^{th} cluster and $\nu_{j,i,k}$ is the delay of the j^{th} ray in the i^{th} cluster relative to $\mu_{i,k}$. The power delay profile of the channel is double exponential decaying by rays and clusters. Since transmitter and receiver are stationary in most PAN applications [14], we assume that the channel remains invariant over a block of symbols.

B. Transmitted Signal

The transmitted signal of the k^{th} user is

$$\tilde{s}^{(k)}(t) = A_k \sum_{i=-\infty}^{\infty} b_i^k x_i^{(k)}(t - iT_r) \tag{2}$$

where T_r is the symbol duration, A_k denotes the amplitude, $b_i^k \in \{\pm 1\}$ is the i^{th} symbol. The i^{th} symbol waveform of the k^{th} user is

$$x_i^{(k)}(t) = \sum_{n=0}^{N_r-1} a_{i,n}^k g^{(k)}(t - nT_c) \tag{3}$$

where N_r is the number of chips in one symbol, $T_c = T_r/N_r$ is the chip duration. Long code is used and $\{a_{i,n}^k\}_{n=0}^{N_r-1}$ is the random DS code assigned to the i^{th} symbol of the k^{th} user. $g^{(k)}(t)$ is the chip waveform formed by passing $z(t)$ through a Prerake filter $\tilde{h}^{(k)}(t)$.

$$g^{(k)}(t) = z(t) * \tilde{h}^{(k)}(t) = \sum_{l=0}^{L_p-1} \tilde{\alpha}_{L_p-1-l,k} z(t - lT_p) \tag{4}$$

where $z(t)$ is an energy-normalized UWB monocycle of duration T_p. The Prerake filter $\tilde{h}^{(k)}(t) = \sum_{l=0}^{L_p-1} \tilde{\alpha}_{L_p-1-l,k}\delta(t - lT_p)$ contains L_p taps. In $\tilde{h}^{(k)}(t)$, $\{\tilde{\alpha}_{l,k}\}_{l=0}^{L_p-1}$ is the estimated value of path gain $\{\alpha_{l,k}\}_{l=0}^{L_p-1}$. The amplitude $A_k = \sqrt{E_p \Big/ \sum_{l=0}^{L_p-1} \mathrm{E}\left[\tilde{\alpha}_{l,k}^2\right]}$ to keep the average transmitted symbol energy constant as $E_b = N_r E_p$.

C. Received Signal

The received signal due to the k^{th} user is given by

$$\begin{aligned} r^{(k)}(t) &= \tilde{s}^{(k)}(t) * h^{(k)}(t) \\ &= A_k \sum_{i=-\infty}^{\infty} b_i^k \underbrace{\left[x_i^{(k)}(t - iT_r) * h^{(k)}(t)\right]}_{\tilde{x}_i^{(k)}(t - iT_r)} \end{aligned} \tag{5}$$

where $\tilde{x}_i^{(k)}(t)$ is obtained using (3) as

$$\begin{aligned} \tilde{x}_i^{(k)}(t) &\triangleq x_i^{(k)}(t) * h^{(k)}(t) \\ &= \sum_{n=0}^{N_r-1} a_{i,n}^k \underbrace{\left[g^{(k)}(t - nT_c) * h^{(k)}(t)\right]}_{\tilde{g}^{(k)}(t - nT_c)} \end{aligned} \tag{6}$$

As shown in (6), $\tilde{g}^{(k)}(t) \triangleq g^{(k)}(t) * h^{(k)}(t)$ is the channel response of a chip waveform $g^{(k)}(t)$.

The total received signal in a K-user system is given by

$$r(t) = \sum_{k=0}^{K-1} r^{(k)}(t - \tau_{0,k}) + n(t) \tag{7}$$

where $n(t)$ is AWGN with double-sided power spectral density of $N_0/2$ and $\tau_{0,k}$ denotes the transmission delay of the k^{th} user. Since random DS codes/data bits are assumed, interfering users appear to the desired user as essentially transmitting random ± 1 sequences and the boundaries of interfering symbols do not matter in asynchronous transmission. This property allows us to assume that $\tau_{0,k}$ is uniformly distributed in $[0, T_c)$.

D. Channel Estimation

The estimated path gain $\{\tilde{\alpha}_{l,k}\}_{l=0}^{L_p-1}$ is obtained by sending N_t pilot pulses $z(t)$. The repetition interval of the pilot pulses is larger than the maximum delay spread of the channel to avoid interference between pilot pulses. During the channel

estimation period of the k^{th} user, all other users keep silent. Assuming perfect synchronization, the base station correlates and samples at the tap rate on the i^{th} received pilot pulse to get estimated path gain on the first L_p paths.

$$\tilde{\alpha}_{l,k}(i)=\int_{lT_p}^{(l+1)T_p}\left(\sum_{l'=0}^{L-1}\alpha_{l',k}z(t-l'T_p)+n_i(t)\right)z(t-lT_p)dt$$

Then N_t estimation results are averaged to obtain the estimated path gain as follows.

$$\tilde{\alpha}_{l,k}=\frac{1}{N_t}\sum_{i=0}^{N_t-1}\tilde{\alpha}_{l,k}(i)=\alpha_{l,k}+n_{l,k} \tag{8}$$

where $n_{l,k}\sim \text{Gaussian}(0,\frac{N_0}{2N_t})$ is the channel estimation noise on the l^{th} path. When $N_t\to\infty$, the variance of $n_{l,k}\to 0$ and channel estimation tends to the perfect estimation.

III. Signal Model and Decision Statistics

A. Signal Structure

Let one chip contain L_c taps, i.e., $T_c=L_cT_p$. The data rate is $R_b=1/(N_rL_cT_p)$. For given N_r and T_p, higher data rate R_b is achieved by decreasing L_c.

In the conventional Partial-Prerake DS UWB system [13], L_c equals to the number of taps in the Prerake filter L_p, and the signal energy captured equals to the maximal ratio combining (MRC) on the first L_p paths. So the captured signal energy in the Partial-Prerake DS UWB system is reduced with the decrease of L_c (or the increase of R_b). As shown in [13], BER performance of the Partial-Prerake DS UWB system degrades rapidly with the growth of data rate.

In this work, we propose to set L_p to a large value while keeping L_c sufficiently small. With a large L_p, more signal energy is captured to guarantee better BER performance. With a small L_c, higher data rate R_b is achieved via superposition of chip waveforms. Comparison of the chip structure in the HDR Prerake and Partial-Prerake schemes is shown in Fig. 1, where the chip duration is fixed by $L_c=4$. As shown, $g^{(k)}(t)$ in the HDR Prerake scheme contains more taps ($L_p=8$) than in the Partial-Prerake scheme ($L_p=4$). The difference between these two schemes is: In the HDR Prerake scheme, the chip waveforms overlap with each other to shorten the chip duration, while in the Partial-Prerake scheme, the chip waveform is tailored to fit the chip duration.

B. Signal Model

The path gain and estimated path gain used in the Prerake filter are defined as vectors $\boldsymbol{\alpha}_k$ and $\tilde{\boldsymbol{\alpha}}_k$ respectively.

$$\begin{aligned}\boldsymbol{\alpha}_k&=\begin{pmatrix}\alpha_{0,k} & \alpha_{1,k} & \cdots & \alpha_{L-1,k}\end{pmatrix}^T\\ \tilde{\boldsymbol{\alpha}}_k&=\begin{pmatrix}\tilde{\alpha}_{L_p-1,k} & \tilde{\alpha}_{L_p-2,k} & \cdots & \tilde{\alpha}_{0,k}\end{pmatrix}^T\end{aligned} \tag{9}$$

Then $\tilde{g}^{(k)}(t)$ in (6) is discretized by $\tilde{g}_{j,k}=\int_{jT_p}^{(j+1)T_p}\tilde{g}^{(k)}(t)z(t-jT_p)dt$ and expressed as

$$\tilde{\mathbf{g}}_k=\mathbf{T}_{\boldsymbol{\alpha}_k}\tilde{\boldsymbol{\alpha}}_k=\begin{pmatrix}\tilde{g}_{0,k} & \tilde{g}_{1,k} & \cdots & \tilde{g}_{L+L_p-2,k}\end{pmatrix}^T \tag{10}$$

where $\mathbf{T}_{\boldsymbol{\alpha}_k}$ is a $(L+L_p-1)\times L_p$ Toeplitz matrix with $\boldsymbol{\alpha}_k$ as the first L elements in its 0^{th} column and zero elsewhere. The effect of imperfect channel estimation is included in $\tilde{\mathbf{g}}_k$ by $\tilde{\boldsymbol{\alpha}}_k$. The element $\tilde{g}_{L_p-1,k}=\sum_{l=0}^{L_p-1}\alpha_{l,k}\tilde{\alpha}_{l,k}$ is the desired peak, which is equivalent to MRC on the first L_p paths. Obviously, larger L_p leads to more signal energy captured. However, overall channel estimation noise increases with the growth of L_p, since total L_p paths are to be estimated and each estimated path gain $\tilde{\alpha}_{l,k}$ contains a noise term $n_{l,k}$ as shown in (8).

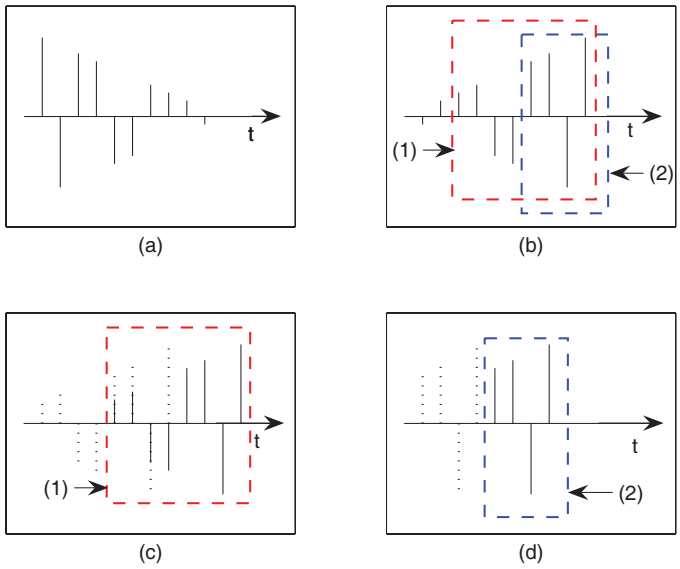

Fig. 1. Comparison of the HDR Prerake and Partial-Prerake schemes, (a) is the channel impulse response $h^{(k)}(t)$ with $L=10$, (b) is the reversal of $h^{(k)}(t)$, where the framed parts (1) and (2) represent $g^{(k)}(t)$ used in the HDR Prerake and Partial-Prerake schemes respectively, (c) is the structure of two chips (one in solid lines, the other in dot lines) in the HDR Prerake scheme, with $L_c=4$, $L_p=8$, (d) is the structure of two chips (one in solid lines, the other in dot lines) in the Partial-Prerake scheme, with $L_c=L_p=4$.

In the HDR Prerake scheme, any chip is interfered by its following n_1 chips and its previous n_2 chips, where $n_1\triangleq\lfloor\frac{L_p-1}{L_c}\rfloor$ and $n_2\triangleq\lfloor\frac{L-1}{L_c}\rfloor$. Assume the n^{th} chip of the i^{th} symbol from the k^{th} user is the desired chip, which has a phase of $a_{i,n}^kb_i^k$. Similarly we can write the phase of each interfering chip as a sequence $\{c_{i,n}^k(0),c_{i,n}^k(1),\cdots,c_{i,n}^k(n_1+n_2)\}$, where $c_{i,n}^k(n_2)=a_{i,n}^kb_i^k$ is the phase of the desired chip. $\{c_{i,n}^k(0),\cdots,c_{i,n}^k(n_2-1)\}$ and $\{c_{i,n}^k(n_2+1),\cdots,c_{i,n}^k(n_1+n_2)\}$ stand for the phases of n_2 and n_1 interfering chips before and after the desired chip respectively.

The received n^{th} chip of the i^{th} symbol from the k^{th} user is expressed as

$$\mathbf{r}_{i,n}^k=\begin{pmatrix}r_{i,n,0}^k & r_{i,n,1}^k & \cdots & r_{i,n,L_c-1}^k\end{pmatrix}^T=A_k\mathbf{T}_{\mathbf{C}_{i,n}^k}\hat{\mathbf{g}}_k \tag{11}$$

Each chip $\mathbf{r}_{i,n}^k$ consists of L_c taps, and the peak is included in the last tap r_{i,n,L_c-1}^k. In (11), $\mathbf{T}_{\mathbf{C}_{i,n}^k}=\mathbf{C}_{i,n}^k\otimes\mathbf{I}_{L_c}$ is a $L_c\times(n_1+n_2+1)L_c$ Toeplitz matrix, $\otimes$ means Kronecker product, $\mathbf{I}_x$ is the identity matrix of size $x\times x$. $\mathbf{C}_{i,n}^k$ is a $1\times(n_1+n_2+1)$ vector built by reversing the phase sequence related to the desired chip as $\mathbf{C}_{i,n}^k=\begin{pmatrix}c_{i,n}^k(n_1+n_2) & c_{i,n}^k(n_1+n_2-1) & \cdots & c_{i,n}^k(0)\end{pmatrix}$. $\hat{\mathbf{g}}_k$ is a $(n_1+n_2+1)L_c\times 1$ vector obtained by extending $\tilde{\mathbf{g}}_k$ as $\hat{\mathbf{g}}_k=\begin{pmatrix}\mathbf{0}_{(n_1+1)L_c-L_p}^T & \tilde{\mathbf{g}}_k^T & \mathbf{0}_{(n_2+1)L_c-L+1}^T\end{pmatrix}^T$, where $\mathbf{0}_x$ denotes the zero row vector with x elements.

C. Decision Statistics

Assume the desired symbol is the 0^{th} symbol of the 0^{th} user. The 0^{th} receiver with perfect synchronization performs correlation on the N_r peaks in the received signal $r(t)$. The output of the 0^{th} receiver is expressed as

$$\begin{aligned} Z &= \underbrace{\int_{(L_p-L_c)T_p}^{(L_p-L_c)T_p+N_rT_c} r^{(0)}(t)v^{(0)}(t)dt}_{S+I_C} \\ &+ \underbrace{\int_{(L_p-L_c)T_p}^{(L_p-L_c)T_p+N_rT_c} \sum_{k=1}^{K-1} r^{(k)}(t-\tau_{0,k})v^{(0)}(t)dt}_{I_M} \\ &+ \underbrace{\int_{(L_p-L_c)T_p}^{(L_p-L_c)T_p+N_rT_c} n(t)v^{(0)}(t)dt}_{N} \end{aligned} \quad (12)$$

where $v^{(0)}(t) = \sum_{n=0}^{N_r-1} a_{0,n}^0 z(t-nT_c-(L_p-1)T_p)$ is the template waveform. Z is decomposed as desired signal S, inter-chip interference I_C, multiple access interference I_M and AWGN term N.

C.1. Desired Signal and Inter-Chip Interference

The sum of S and I_C is given by

$$S+I_C=\sum_{n=0}^{N_r-1}\underbrace{\int_{(L_p-L_c)T_p+nT_c}^{(L_p-L_c)T_p+(n+1)T_c} r^{(0)}(t)a_{0,n}^0 z(t-nT_c-(L_p-1)T_p)dt}_{S(n)+I_C(n)} \quad (13)$$

As shown in (13), detection of a symbol is decomposed as detection of N_r chips. In the n^{th} chip detection, $S(n)$ and $I_C(n)$ is expressed as

$$\begin{aligned} S(n)+I_C(n) &= \mathbf{v}_{0,n}^0\mathbf{r}_{0,n}^0 \\ &= \underbrace{A_0\mathbf{v}_{0,n}^0\mathbf{T}_{\mathbf{C}_{0,n}^0}\hat{\mathbf{g}}_0'}_{S(n)} + \underbrace{A_0\mathbf{v}_{0,n}^0\mathbf{T}_{\mathbf{C}_{0,n}^0}(\hat{\mathbf{g}}_0-\hat{\mathbf{g}}_0')}_{I_C(n)} \end{aligned} \quad (14)$$

where $\mathbf{v}_{0,n}^0 = \begin{pmatrix} \mathbf{0}_{L_c-1} & a_{0,n}^0 \end{pmatrix}$ is the discrete format of the template waveform in the n^{th} chip detection. Since $\tilde{g}_{L_p-1,0}$ is the peak containing the desired signal energy, $\hat{\mathbf{g}}_0'$ is obtained by setting all elements in $\hat{\mathbf{g}}_0$ as zeros except the element $\tilde{g}_{L_p-1,0}$.

C.2. Multiple Access Interference

In the pervious work on Prerake TDD CDMA [3], imperfect channel estimation in MAI has been neglected to avoid computational complexity. However, imperfect channel estimation affects the statistical property of MAI. For completeness, we consider the effect of imperfect channel estimation in I_M in this paper. From (12), I_M is given by

$$I_M=\sum_{k=1}^{K-1}\sum_{n=0}^{N_r-1}\underbrace{\int_{(L_p-L_c)T_p+nT_c}^{(L_p-L_c)T_p+(n+1)T_c} r^{(k)}(t-\tau_{0,k})a_{0,n}^0 z(t-nT_c-(L_p-1)T_p)dt}_{I_M^k(n)} \quad (15)$$

where $I_M^k(n)$ is the interference from the k^{th} interfering user in the n^{th} chip detection.

The asynchronous delay $\tau_{0,k}$ is split as $\tau_{0,k} = \gamma_k T_p + \Delta T_k$, where $\gamma_k \in \{0, 1, \cdots, L_c-1\}$ and $\Delta T_k \in [0, T_p)$, both with uniform distribution. The partial autocorrelation function of $z(t)$ is defined as $P(x) = \int_0^x z(t)z(t+T_p-x)\,dt$. Then $I_M^k(n)$ is expressed as

$$\begin{aligned} I_M^k(n) &= \mathbf{v}_{0,n}^0\mathbf{r}_{0,n}^k(\gamma_k+1)P(\Delta T_k) \\ &\quad + \mathbf{v}_{0,n}^0\mathbf{r}_{0,n}^k(\gamma_k)P(T_p-\Delta T_k) \end{aligned} \quad (16)$$

where $\mathbf{r}_{0,n}^k(x) =$

$$\begin{aligned} &\left(r_{0,n-1,L_c-x}^k \cdots r_{0,n-1,L_c-1}^k\, r_{0,n,0}^k \cdots r_{0,n,L_c-1-x}^k\right)^T, n\neq 0 \\ &\left(r_{-1,N_r-1,L_c-x}^k \cdots r_{-1,N_r-1,L_c-1}^k\, r_{0,0,0}^k \cdots r_{0,0,L_c-1-x}^k\right)^T, n=0 \end{aligned} \quad (17)$$

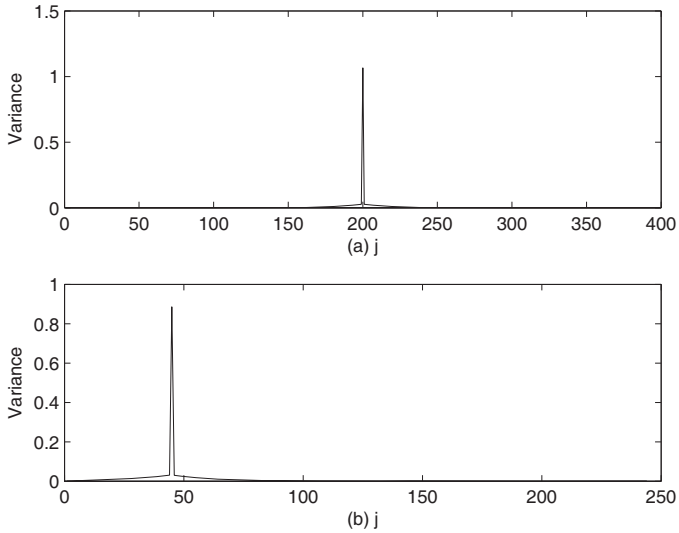

Fig. 2. The variance of $\tilde{g}_{j,k}$, (a) is in CM1, $L_p = 200$ with perfect channel estimation ($N_t = \infty$), (b) is in CM1, $L_p = 45$ with imperfect channel estimation ($N_t = 200$).

IV. Distribution of Interference

In (14), it is observed that $I_C(n)$ is a summation of $\tilde{g}_{j,0}$ with random phases, where $j = L_p - 1 + xL_c$, $x \in \{-n_1, \cdots, n_2\}$ and $x \neq 0$ (which means the peak $\tilde{g}_{L_p-1,0}$ is not included). Similarly, it is observed from (16) and (17) that $I_M^k(n)$ is a summation of elements in $\tilde{\mathbf{g}}_k$ sampled by the interval of L_c with random phases and the partial autocorrelation effect. Because of the asynchronous delay $\tau_{0,k}$, $I_M^k(n)$ contains the peak $\tilde{g}_{L_p-1,k}$. Then I_C and I_M are obtained by summation of $I_C(n)$ and $I_M^k(n)$ respectively.

The distribution of I_C and I_M depends on the distribution of $\tilde{g}_{j,k}$. The variance of $\tilde{g}_{j,k}$ under both perfect and imperfect channel estimation is plotted in Fig. 2, which reflects signal energy focusing in the received Prerake UWB signals. In both cases, the peak $\tilde{g}_{L_p-1,k}$ has a noticeably large variance, while the variance of non-peaks $\tilde{g}_{j,k}$ with $j \neq L_p - 1$ is much smaller.

Since I_C does not contain the peak, all terms in the summation are with relatively similar variance. Therefore I_C can be approximated as a Gaussian random variable using Central Limit Theorem (CLT). In contrast, I_M contains the peak $\tilde{g}_{L_p-1,k}$, which is a dominant term in the summation because of its distinguishing variance. And the Gaussian distribution does not well fit the distribution of I_M because the basis of CLT is violated. Therefore, we propose to use a more

appropriate model, the generalized Gaussian distribution, to fit the distribution of I_M.

In the Appendix, evaluation of the expectation values related to $\tilde{g}_{j,k}$ is provided, which will be used in the derivation of variance and higher order moment of I_C and I_M.

A. Inter-Chip Interference

Since I_C is modeled as a Gaussian random variable, we need to evaluate its mean and variance. It is easy to show the mean of $\{I_C(n)\}_{n=0}^{N_r-1}$ is zero and for different n, $I_C(n)$ are independent conditioned on $\boldsymbol{\alpha}_0$ and $\tilde{\boldsymbol{\alpha}}_0$. Therefore the mean of I_C is zero. The variance of I_C conditioned on $\boldsymbol{\alpha}_0$ and $\tilde{\boldsymbol{\alpha}}_0$ is given by

$$\begin{aligned}\sigma^2_{I_C} &= N_r\sigma^2_{I_C(n)}\\ &= N_r A_0^2 \mathrm{E}\Big[\mathbf{v}^0_{0,n}\mathbf{T}_{\mathbf{C}^0_{0,n}}(\hat{\mathbf{g}}_0-\hat{\mathbf{g}}'_0)(\hat{\mathbf{g}}_0-\hat{\mathbf{g}}'_0)^T\mathbf{T}^T_{\mathbf{C}^0_{0,n}}(\mathbf{v}^0_{0,n})^T\Big]\\ &= N_r A_0^2 \sum_{\substack{x=-n_2\\ x\neq 0}}^{n_1} \tilde{g}^2_{L_p-1-xL_c,0} \end{aligned} \tag{18}$$

B. Multiple Access Interference

As well as I_C, it is easy to find the mean of I_M is zero. Since the peak $\tilde{g}_{L_p-1,k}$ is a dominant term in $I^k_M(n)$, we use a generalized Gaussian distribution [16] to fit the distribution of I_M instead of the conventionally used Gaussian distribution[2]. The probability density function (PDF) of a zero mean generalized Gaussian random variable x is

$$f_X(x) = a\exp(-b^\zeta|x|^\zeta), \quad -\infty < x < \infty, \quad \zeta > 0 \tag{19}$$

where $a = \sqrt{\frac{b\zeta}{2\Gamma(1/\zeta)}}$, $b = \frac{1}{\sigma}\sqrt{\frac{\Gamma(3/\zeta)}{\Gamma(1/\zeta)}}$, σ^2 is the variance of x, ζ denotes the shape parameter, and $\Gamma(z) = \int_0^\infty t^{z-1}e^{-t}dt$. When $\zeta = 1$ and 2, $f_X(x)$ is reduced to its special cases of Laplace and Gaussian PDF respectively.

To evaluate the parameter ζ in (19), the moment matching method with kurtosis ratio is adopted [18]. The n^{th} moment of the zero mean generalized Gaussian distribution is given by

$$\mathrm{E}[x^n] = \begin{cases} 0 & n = 1,3,5,\cdots \\ \sigma^n \frac{\Gamma((n+1)/\zeta)}{\Gamma^{n/2}(3/\zeta)\Gamma^{1-n/2}(1/\zeta)} & n = 2,4,6,\cdots \end{cases} \tag{20}$$

Substitute (20) into the definition of kurtosis, we get

$$\mathcal{K}(\zeta) = \frac{\mathrm{E}[x^4]}{(\mathrm{E}[x^2])^2} = \frac{\Gamma(5/\zeta)\Gamma(1/\zeta)}{\Gamma^2(3/\zeta)} \tag{21}$$

To determine the distribution of I_M, we calculate the variance and 4^{th} moment of I_M and substitute them into (21) to find the generalized Gaussian distribution parameter ζ. We compute the variance and 4^{th} moment of $I^k_M(n)$ first, and then extend the results to obtain the variance and 4^{th} moment of I_M.

[2]In a recent work on TH UWB system [17], coincidentally, the Laplace distribution is adopted to model MAI, which is a special case of the zero mean generalized Gaussian distribution.

The variance of $I^k_M(n)$ is evaluated as

$$\begin{aligned}\sigma^2_{I^k_M(n)} &= \frac{2}{L_c}\mathrm{E}\left[P^2(\Delta T_k)\right]\mathrm{E}\left[(\mathbf{r}^k_{i,n})^T\mathbf{r}^k_{i,n}\right]\\ &= \frac{2A_k^2}{L_c}\mathrm{E}\left[P^2(\Delta T_k)\right]\sum_{j=0}^{L+L_p-2}\mathrm{E}\left[\tilde{g}^2_{j,k}\right]\end{aligned} \tag{22}$$

The variance of I_M is given by

$$\sigma^2_{I_M} = (K-1)\sigma^2_{I^k_M} = (K-1)N_r\sigma^2_{I^k_M(n)} \tag{23}$$

The 4^{th} moment of $I^k_M(n)$ is evaluated by

$$\begin{aligned}&\mathrm{E}\Big[\big(I^k_M(n)\big)^4\Big] = \tfrac{2}{L_c}\mathrm{E}\big[P^4(\Delta T_k)\big]\,\mathrm{E}\Big[\sum_{m=0}^{L_c-1}(r^k_{i,n,m})^4\Big]\\ &= \tfrac{2A_k^4}{L_c}\mathrm{E}\big[P^4(\Delta T_k)\big]\sum_{j=0}^{L+L_p-2}\mathrm{E}\Big[\tilde{g}^4_{j,k}\Big]\\ &+\tfrac{6A_k^4}{L_c}\mathrm{E}\big[P^4(\Delta T_k)\big]\sum_{m=0}^{L_c-1}\sum_x\sum_{x'}\mathrm{E}\Big[\tilde{g}^2_{L_p+xL_c+m,k}\tilde{g}^2_{L_p+x'L_c+m,k}\Big]\end{aligned}$$

where both x and x' sum from $-(n_1+1)$ to (n_2-1), and $x' \neq x$.

The 4^{th} moment of I^k_M is calculated as

$$\begin{aligned}&\mathrm{E}\Big[\big(I^k_M\big)^4\Big] = \tfrac{2A_k^4(N_r+3N_r(N_r-1))}{L_c}\mathrm{E}\big[P^4(\Delta T_k)\big]\,\mathrm{E}\Big[\tilde{g}^4_{j,k}\Big]\\ &+\tfrac{6A_k^4N_r^2}{L_c}\mathrm{E}\big[P^4(\Delta T_k)\big]\sum_{m=0}^{L_c-1}\sum_x\sum_{x'}\mathrm{E}\Big[\tilde{g}^2_{L_p+xL_c+m,k}\tilde{g}^2_{L_p+x'L_c+m,k}\Big]\end{aligned}$$

where both x and x' sum from $-(n_1+1)$ to (n_2-1), and $x' \neq x$.

The 4^{th} moment of I_M is obtained by

$$\mathrm{E}\Big[(I_M)^4\Big] = (K-1)\mathrm{E}\Big[\big(I^k_M\big)^4\Big] + 3(K-1)(K-2)N_r\sigma^2_{I^k_M(n)}$$

V. BER Performance Analysis

Denote the total noise $\iota = I_C + I_M + N$, where I_C, I_M and N are independent. The CF method [19] [20] is used to derive the BER formula.

The characteristic function of ι is given by

$$\Phi_\iota(\omega) = \underbrace{2\int_0^\infty a\exp\big(-b^\zeta m^\zeta\big)\cos(\omega m)dm}_{\Phi_{I_M}(\omega)} \cdot \underbrace{\exp\left(-\frac{\omega^2(\sigma^2_{I_C}+\sigma^2_N)}{2}\right)}_{\Phi_{I_C+N}(\omega)}$$

where $\Phi_{I_M}(\omega)$ and $\Phi_{I_C+N}(\omega)$ represent the characteristic functions of I_M and $I_C + N$ respectively. And $\Phi_{I_M}(\omega)$ is obtained by taking a Fourier transform on (19).

The instantaneous BER is derived as

$$\begin{aligned}P_{\text{Instant}} &= \frac{1}{2} - \int_0^{|S|}\underbrace{\frac{1}{2\pi}\int_{-\infty}^{\infty}\Phi_\iota(\omega)\exp(-j\omega x)d\omega}_{\text{PDF of }\iota}\,dx\\ &= \frac{1}{2} - \frac{a}{2}\int_0^\infty \exp\big(-b^\zeta m^\zeta\big)\,\mathrm{erf}\left(\frac{m+|S|}{\sqrt{2(\sigma^2_{I_C}+\sigma^2_N)}}\right)dm\\ &\quad -\frac{a}{2}\int_0^{|S|}\exp\big(-b^\zeta m^\zeta\big)\,\mathrm{erf}\left(\frac{|S|-m}{\sqrt{2(\sigma^2_{I_C}+\sigma^2_N)}}\right)dm\\ &\quad +\frac{a}{2}\int_{|S|}^\infty \exp\big(-b^\zeta m^\zeta\big)\,\mathrm{erf}\left(\frac{m-|S|}{\sqrt{2(\sigma^2_{I_C}+\sigma^2_N)}}\right)dm\end{aligned} \tag{24}$$

TABLE I
THE PARAMETERS USED IN NUMERICAL STUDY

Model Parameters	CM1	CM3
Γ_1 (cluster power decay factor)	7.1	14
Γ_2 (ray power decay factor)	4.3	7.9
σ_1 (stand. dev. of cluster lognormal fading in dB)	3.3941	3.3941
σ_2 (stand. dev. of ray lognormal fading in dB)	3.3941	3.3941
L (path number)	200	400

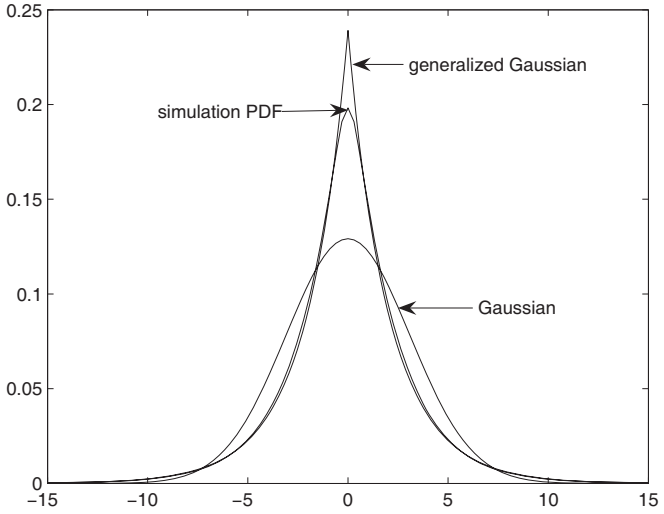

Fig. 3. The simulation PDF of I_M, its generalized Gaussian fitting and its Gaussian fitting in CM3, $L_p = 125$, $L_c = 5$, $R_b = 25$Mbps, imperfect channel estimation ($N_t = 200$), 4 users.

where $S = N_r S(n) = N_r A_0 b_0^0 \tilde{g}_{L_p-1,0}$ is the desired signal defined in (12). The average BER is computed by averaging P_{Instant} over the lognormal fading channel using the Monte Carlo method.

VI. Numerical Results and Discussion

According to [14], channel parameters are listed in Table I. The UWB monocycle is $z(t) = \varepsilon \left[1 - 4\pi \left(\frac{t - T_p/2}{\tau_p}\right)^2\right] \exp\left[-2\pi \left(\frac{t - T_p/2}{\tau_p}\right)^2\right]$, where $T_p = 0.25$ns, $\tau_p = 0.10275$ns and $\varepsilon = 1.6111 \times 10^5$. The length of the DS code is set as $N_r = 32$. System performance is studied under the data rate of $R_b = 25$Mbps (i.e., $L_c = 5$).

A. Distribution of Interference

In Fig. 3 and Fig. 4, the simulation PDFs of I_M and I_C are plotted respectively, where the channel is CM3, the number of users $K = 4$, $L_p = 125$, $R_b = 25$Mbps, under imperfect channel estimation with $N_t = 200$.

In Fig. 3, the generalized Gaussian fitting and Gaussian fitting for the PDF of I_M is given to compare with the simulation PDF of I_M. It is clearly shown that the generalized Gaussian distribution fits the simulation PDF of I_M much more accurately than the Gaussian distribution in most value range. Though the generalized Gaussian distribution does not match well with the simulation PDF at the center (i.e., around 0), it should be emphasized that the tail of the interference distribution is of the most important interest in BER calculation (involving the tail integral) especially when SNR is medium or high. Therefore the mismatch around the center does not affect much in the BER performance evaluation.

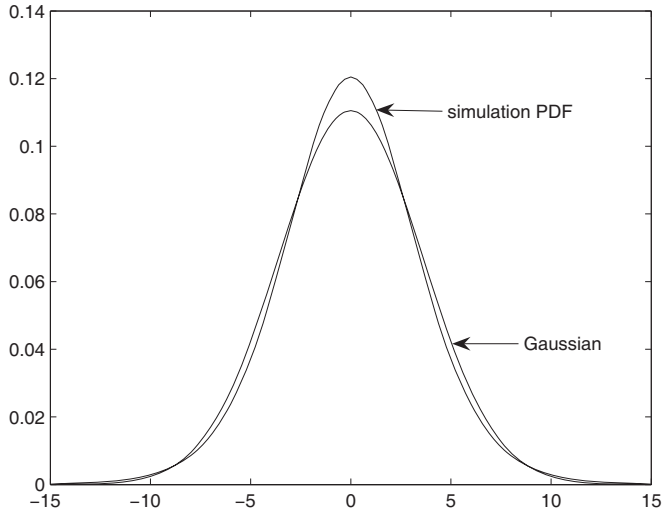

Fig. 4. The simulation PDF of I_C and its Gaussian fitting in CM3, $L_p = 125$, $L_c = 5$, $R_b = 25$Mbps, imperfect channel estimation ($N_t = 200$), 4 users.

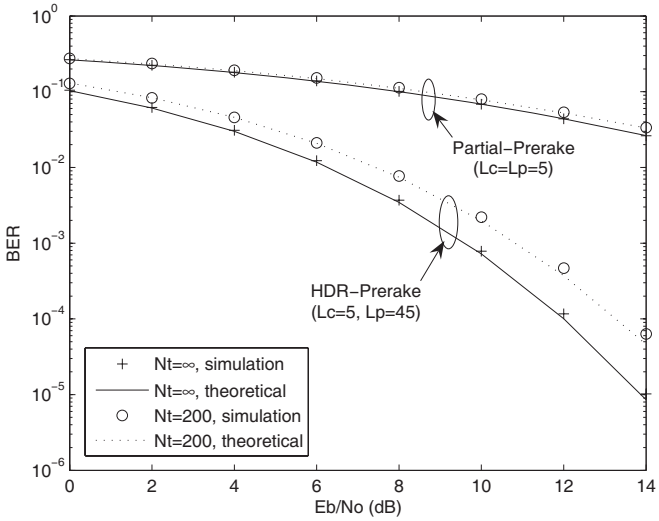

Fig. 5. BER performance comparison of the HDR Prerake DS UWB system and the Partial-Prerake DS UWB system in CM1, $R_b = 25$Mbps, under both perfect ($N_t = \infty$) and imperfect channel estimation ($N_t = 200$), 1 user.

In Fig. 4, the Gaussian fitting for the PDF of I_C is provided to compare with the simulation PDF of I_C. It is observed the simulation PDF of I_C almost fits well with the Gaussian distribution, which means that I_C can be well approximated as a Gaussian random variable.

B. BER Performance

In Fig. 5, BER performance comparison of the HDR Prerake DS UWB system and the Partial-Prerake DS UWB system is provided in a single user scenario. The data rate of these two systems is the same as $R_b = 25$Mbps (i.e., $L_c = 5$). It is observed that the HDR Prerake DS UWB system significantly outperforms the Partial-Prerake DS UWB system under both

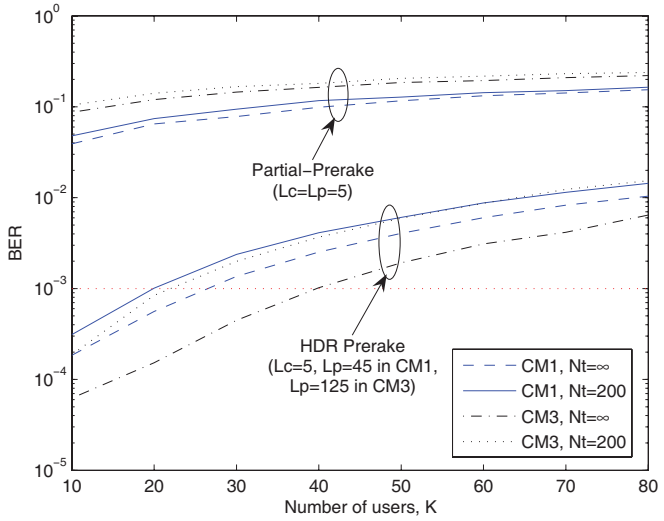

Fig. 6. Multiple access performance of the HDR Prerake DS UWB system and the Partial-Prerake DS UWB system under perfect ($N_t = \infty$) and imperfect channel estimation ($N_t = 200$), $R_b = 25$Mbps, $L_c = 5$, $E_b/N_0 = 16dB$.

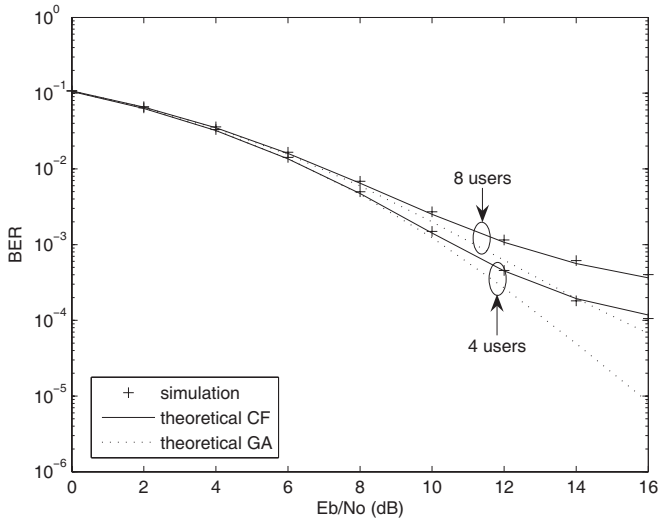

Fig. 7. Comparison of the accuracy of the GA and CF methods in BER calculation under perfect channel estimation ($N_t = \infty$) in CM1, $R_b = 25$Mbps, $L_c = 5$, $L_p = 45$, the number of users $K = 4$ and 8 respectively.

perfect and imperfect channel estimation. The reason lies in the different amount of signal energy captured in these two systems. In the Partial-Prerake DS UWB system, $L_p = L_c = 5$ means that the signal energy on the first 5 paths are captured only (around 25% of the total signal energy). In contrast, we set $L_p = 45 > L_c$ in the HDR Prerake DS UWB system. So the signal energy on the first 45 paths are captured (around 90% of the total signal energy).

In Fig. 6, multiple access performance of the HDR Prerake and Partial-Prerake DS UWB systems is compared under a fixed transmission SNR of $E_b/N_0 = 16$dB. The data rate is set as $R_b = 25$Mbps. It is shown that overall BER performance of the Partial-Prerake DS UWB system is unacceptable due to insufficient signal energy captured. On the contrary, the HDR Prerake DS UWB system can support up to 27 and 40 users in CM1 and CM3 respectively, with a desired BER

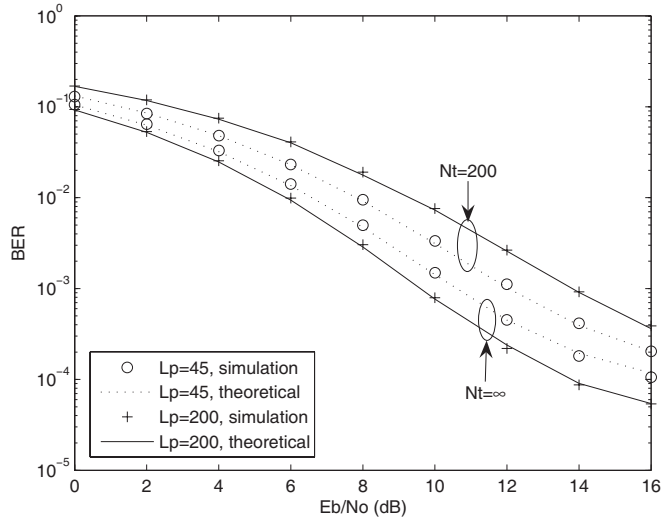

Fig. 8. The effect of imperfect channel estimation ($N_t = 200$) with different number of taps L_p in Prerake filter in CM1, $R_b = 25$Mbps, $L_c = 5$, 4 users.

value of 10^{-3}. Overall BER performance in an acceptable range (i.e., BER$\leq 10^{-3}$) in CM3 is better than in CM1, which is consistent with the results in [13]. This also implies that better multiple access performance can be achieved in a denser multipath environment because of the higher degree of the multipath diversity.

In Fig. 7, comparison of the accuracy of the CF and Gaussian Approximation (GA) methods in BER calculation is provided in CM1 with the number of user $K = 4$ and 8. The theoretical BER curve calculated using the CF method (refer to (24)) matches well with the simulation results. In contrast, the theoretical BER curve computed using the GA method [20] (i.e., I_M is approximated as a Gaussian random variable) deviates from the simulation results in medium and high E_b/N_0 range. Fig. 7 justifies the rationality of the generalized Gaussian distribution assumption for the distribution of MAI from another viewpoint, which is consistent with Fig. 3.

C. Tradeoff Between Energy Capture and Imperfect Channel Estimation Effect

In Fig. 8, the effect of imperfect channel estimation is illustrated. The number of taps in the Prerake filter takes two values: $L_p = 45$ and 200. When $L_p = 45$, around 90% of the total signal energy is captured. On the other hand, $L_p = 200$ means signal energy on all paths (100%) is captured. Under perfect channel estimation ($N_t = \infty$), $L_p = 200$ gives better BER performance because of more signal energy captured. In contrast, $L_p = 45$ yields better BER performance in case of imperfect channel estimation ($N_t = 200$). This observation suggests that, under imperfect channel estimation, BER performance is affected by both the signal energy captured and the channel estimation noise. For each estimated path, a channel estimation noise term $n_{l,k}$ is added (as shown in (8)). With the growth of L_p, the channel estimation noise is increased as well as the signal energy captured. Hence there is a tradeoff between the signal energy capture and the channel estimation noise.

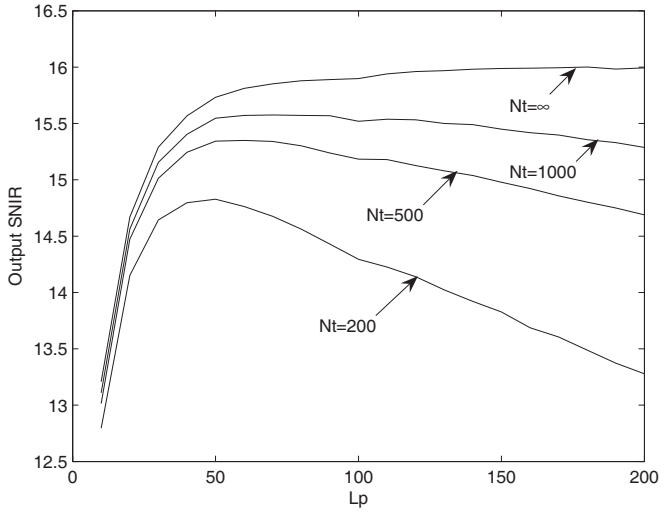

Fig. 9. The output SNIR as a function of number of taps L_p in the Prerake filter under perfect ($N_t = \infty$) and imperfect channel estimation ($N_t = 200, 500, 1000$) with $E_b/N_0 = 16$dB in CM1, $R_b = 25$Mbps, $L_c = 5$, 4 users.

In Fig. 9, the output SNIR $S^2/\left(\sigma_{I_C}^2 + \sigma_{I_M}^2 + \sigma_N^2\right)$ is plotted versus the number of taps L_p in the Prerake filter. Four different values of N_t are used: $N_t = 200, 500, 1000, \infty$. The larger value of N_t means that the smaller channel estimation noise $n_{l,k}$ is added to each estimated path (refer to (8)). As a result, larger N_t brings overall higher output SNIR. One important finding is that the output SNIR is a convex function of L_p under imperfect channel estimation ($N_t \neq \infty$) and an optimal L_p exists. This can be explained by the tradeoff between the signal energy captured and the channel estimation noise. Since the power decay profile of UWB channels is double exponential decaying by rays and clusters, the signal energy captured does not increase linearly with the growth of L_p. On the other hand, the channel estimation noise is linearly proportional to L_p. Therefore in a practical system design, appropriate value of L_p should be chosen to capture enough signal energy while keeping the effect of imperfect channel estimation tolerable. Though the theoretical derivation of optimal L_p is intractable, it is found that 90% signal energy capturing is a good choice for Prerake filter design in our extensive experiments.

VII. Conclusions

A novel HDR Prerake DS UWB multiple access system is proposed. Its main advantage is that high data rate can be achieved without sacrificing the signal energy captured. Simulation results show that the HDR Prerake DS UWB system significantly outperforms the conventional Partial-Prerake DS UWB system in high data rate scenarios. Next, a more appropriate statistical model, the generalized Gaussian distribution, is proposed for the distribution of MAI. Based on this model, the BER formula is derived using the CF method. The accuracy of the BER formula is verified by numerical results. Then the effect of imperfect channel estimation is studied. We highlight the tradeoff between signal energy captured and the imperfect channel estimation effect. In a practical system design, the number of taps in the Prerake filter should be chosen to capture enough signal energy while keeping the effect of imperfect channel estimation tolerable.

Appendix

All the expectation values related to $\tilde{g}_{j,k}$ are derived using the following convolution. To simplify the notation, we will drop the user index k in the following derivation of expectation values.

$$\begin{aligned}\tilde{g}_{j,k} &= \sum_{n=\max[0,j-L+1]}^{\min[j,L_p-1]} \alpha_{j-n,k}\tilde{\alpha}_{L_p-1-n,k} \\ &= \sum_{n=\max[0,j-L+1]}^{\min[j,L_p-1]} \alpha_{j-n,k}\left(\alpha_{L_p-1-n,k} + n_{L_p-1-n,k}\right) \quad (25)\end{aligned}$$

In the derivations, the x^{th} (where x is an even number) moment of $\alpha_{l,k}$ is obtained by the x^{th} moment of $\beta_{l,k}$, i.e., $\mathrm{E}[(\beta_{l,k})^x] = \exp(x\eta_{y_{l,k}} + x^2\sigma_{y_{l,k}}^2/2)$, where $\beta_{l,k} = \exp(y_{l,k})$ and $y_{l,k} \sim \mathrm{Gaussian}(\eta_{y_{l,k}}, \sigma_{y_{l,k}}^2)$.

A. The 2nd Moment

A.1. $j \neq L_p - 1$

$$\mathrm{E}\left[\tilde{g}_j^2\right] = \sum_{n=\max[0,j-L+1]}^{\min[j,\,L_p-1]} \mathrm{E}\left[\alpha_{j-n}^2\right]\mathrm{E}\left[\alpha_{L_p-1-n}^2\right] + \frac{N_0}{2N_t}\sum_{n=\max[0,j-L+1]}^{\min[j,\,L_p-1]} \mathrm{E}\left[\alpha_{j-n}^2\right]$$

A.2. $j = L_p - 1$

$$\mathrm{E}\left[\tilde{g}_j^2\right] = \sum_{n=0}^{L_p-1} \mathrm{E}\left[\alpha_n^4\right] + \sum_{n=0}^{L_p-1}\sum_{\substack{n'=0\\n'\neq n}}^{L_p-1} \mathrm{E}\left[\alpha_n^2\right]\mathrm{E}\left[\alpha_{n'}^2\right] + \frac{N_0}{2N_t}\sum_{n=0}^{L_p-1}\mathrm{E}\left[\alpha_n^2\right]$$

B. The 4th Moment

B.1. $j \neq L_p - 1$

The range of n and m in the following summation is $\{\max[0, j-L+1], \cdots, \min[j, L_p-1]\}$. To simplify the expression, we define $f_1 = j-n$, $f_2 = L_p-1-n$, $f_3 = j-m$ and $f_4 = L_p - 1 - m$.

$$\begin{aligned}\mathrm{E}\left[\tilde{g}_j^4\right] =& \sum_n \mathrm{E}\left[\alpha_{f_1}^4\right]\mathrm{E}\left[\alpha_{f_2}^4\right] + \frac{3N_0}{Nt}\sum_n \mathrm{E}\left[\alpha_{f_1}^4\right]\mathrm{E}\left[\alpha_{f_2}^2\right] \\ &+3\sum_n \sum_{\substack{m,m\neq n\\ f_1\neq f_4, f_2\neq f_3}} \mathrm{E}\left[\alpha_{f_1}^2\right]\mathrm{E}\left[\alpha_{f_2}^2\right]\mathrm{E}\left[\alpha_{f_3}^2\right]\mathrm{E}\left[\alpha_{f_4}^2\right] \\ &+3\sum_n \sum_{\substack{m,m\neq n\\ f_1=f_4}} \mathrm{E}\left[\alpha_{f_1}^4\right]\mathrm{E}\left[\alpha_{f_2}^2\right]\mathrm{E}\left[\alpha_{f_3}^2\right] \\ &+3\sum_n \sum_{\substack{m,m\neq n\\ f_2=f_3}} \mathrm{E}\left[\alpha_{f_1}^2\right]\mathrm{E}\left[\alpha_{f_3}^4\right]\mathrm{E}\left[\alpha_{f_4}^2\right] \\ &+\frac{3N_0^2}{4N_t^2}\sum_n \mathrm{E}\left[\alpha_{f_1}^4\right] + \frac{3N_0^2}{4N_t^2}\sum_n \sum_{\substack{m\\ m\neq n}} \mathrm{E}\left[\alpha_{f_1}^2\right]\mathrm{E}\left[\alpha_{f_3}^2\right] \\ &+\frac{3N_0}{Nt}\sum_n \sum_{\substack{m,m\neq n\\ f_2\neq f_3}} \mathrm{E}\left[\alpha_{f_1}^2\right]\mathrm{E}\left[\alpha_{f_2}^2\right]\mathrm{E}\left[\alpha_{f_3}^2\right] \\ &+\frac{3N_0}{Nt}\sum_n \sum_{\substack{m,m\neq n\\ f_2=f_3}} \mathrm{E}\left[\alpha_{f_1}^2\right]\mathrm{E}\left[\alpha_{f_3}^4\right]\end{aligned}$$

B.2. $j = L_p - 1$

The range of n and m in the following summation is $\{0, \cdots, L_p - 1\}$.

$$\begin{aligned}
\mathrm{E}\big[\tilde{g}_j^4\big] = &\sum_n \mathrm{E}\big[\alpha_n^8\big] + 3\sum_n \sum_{\substack{m \\ m\neq n}} \mathrm{E}\big[\alpha_n^4\big]\,\mathrm{E}\big[\alpha_m^4\big] \\
&+6\sum_n \sum_{\substack{m \\ m\neq n}} \sum_{\substack{l,l\neq n \\ l\neq m}} \mathrm{E}\big[\alpha_n^2\big]\,\mathrm{E}\big[\alpha_m^2\big]\,\mathrm{E}\big[\alpha_l^4\big] \\
&+\sum_n \sum_{\substack{m \\ m\neq n}} \sum_{\substack{l,l\neq n \\ l\neq m}} \sum_{\substack{p,p\neq n \\ p\neq m, p\neq l}} \mathrm{E}\big[\alpha_n^2\big]\,\mathrm{E}\big[\alpha_m^2\big]\,\mathrm{E}\big[\alpha_l^2\big]\,\mathrm{E}\big[\alpha_p^2\big] \\
&+4\sum_n \sum_{\substack{m \\ m\neq n}} \mathrm{E}\big[\alpha_n^2\big]\,\mathrm{E}\big[\alpha_m^6\big] \\
&+\frac{3N_0^2}{4N_t^2}\sum_n \mathrm{E}\big[\alpha_n^4\big] + \frac{3N_0^2}{4N_t^2}\sum_n \sum_{\substack{m \\ m\neq n}} \mathrm{E}\big[\alpha_n^2\big]\,\mathrm{E}\big[\alpha_m^2\big] \\
&+\frac{3N_0}{N_t}\sum_n \mathrm{E}\big[\alpha_n^6\big] + \frac{9N_0}{N_t}\sum_n \sum_{\substack{m \\ m\neq n}} \mathrm{E}\big[\alpha_n^4\big]\,\mathrm{E}\big[\alpha_m^2\big] \\
&+\frac{3N_0}{N_t}\sum_n \sum_{\substack{m \\ m\neq n}} \sum_{\substack{l,l\neq n \\ l\neq m}} \mathrm{E}\big[\alpha_n^2\big]\,\mathrm{E}\big[\alpha_m^2\big]\,\mathrm{E}\big[\alpha_l^2\big]
\end{aligned}$$

C. Expectation of Square Product

It is assumed that $j_1 \neq j_2$. The range of n in the following summation is $\{\max[0, j_1 - L + 1], \cdots, \min[j_1, L_p - 1]\}$. And the range of m is $\{\max[0, j_2 - L + 1], \cdots, \min[j_2, L_p - 1]\}$.

$$\begin{aligned}
\mathrm{E}\big[\tilde{g}_{j_1}^2\,\tilde{g}_{j_2}^2\big] = &\mathrm{E}\left[\left(\sum_n \alpha_{j_1-n}\alpha_{L_p-1-n}\right)^2\left(\sum_m \alpha_{j_2-m}\alpha_{L_p-1-m}\right)^2\right] \\
&+\frac{N_0}{2N_t}\mathrm{E}\left[\sum_n\sum_m \alpha_{j_1-n}^2\alpha_{L_p-1-n}^2\alpha_{j_2-m}^2\right] \\
&+\frac{N_0}{2N_t}\mathrm{E}\left[\sum_n\sum_m \alpha_{j_1-n}^2\alpha_{j_2-m}^2\alpha_{L_p-1-m}^2\right] \\
&+\mathrm{E}\left[\left(\sum_n \alpha_{j_1-n}n_{L_p-1-n}\right)^2\left(\sum_m \alpha_{j_2-m}n_{L_p-1-m}\right)^2\right]
\end{aligned}$$

REFERENCES

[1] M. Z. Win and R. A. Scholtz, "Ultra-wide bandwidth time-hopping spread-spectrum impulse radio for wireless multiple-access communications," *IEEE Trans. Commun*, vol. 48, no. 4, pp. 679–689, Apr. 2000.

[2] ——, "On the energy capture of ultrawide bandwidth signals in dense multipath environments," *IEEE Commun. Lett.*, vol. 2, no. 9, pp. 245–247, Sept. 1998.

[3] S. E. El-Khamy, E. E. Sourour, and T. A. Kadous, "Wireless portable communications using pre-RAKE CDMA/TDD/QPSK systems with different combining techniques and imperfect channel estimation," in *Proc. IEEE PIMRC 1997*, Sept. 1997, pp. 529–533.

[4] R. Esmailzadeh, E. Sourour, and M. Nakagawa, "PreRAKE diversity combining in time-division duplex CDMA mobile communications," *IEEE Trans. Veh. Technol.*, vol. 48, no. 3, pp. 795–801, May 1999.

[5] N. Guo, R. C. Qiu, and B. M. Sadler, "An ultra-wideband autocorrelation demodulation scheme with low-complexity time reversal enhancement," in *Proc. MILCOM 2005*, Oct. 2005, pp. 1–7.

[6] T. Strohmer, M. Emami, J. Hansen, G. Papanicolaou, and A. J. Paulraj, "Application of time-reversal with MMSE equalizer to UWB communications," in *Proc. IEEE GLOBECOM*, Nov. 2004, pp. 3123–3127.

[7] G. F. Edelmann, H. C. Song, S. Kim, W. S. Hodgkiss, W. A. Kuperman, and T. Akal, "Underwater acoustic communications using time reversal," *IEEE J. Oceanic Engineering*, vol. 30, no. 4, pp. 852–864, Oct. 2005.

[8] S. Imada and T. Ohtsuki, "Pre-RAKE diversity combining for UWB systems in IEEE 802.15 UWB multipath channel," in *Proc. Joint UWBST and IWUWBS*, May 2004, pp. 236–240.

[9] K. Usuda, H. Zhang, and M. Nakagawa, "Pre-RAKE diversity combining for UWB systems in IEEE 802.15 UWB multipath channel," in *Proc. IEEE WCNC*, May 2004, pp. 236–240.

[10] M. Emami, M. Vu, J. Hansen, A. J. Paulraj, and G. Papanicolaou, "Matched filtering with rate back-off for low complexity communications in very large delay spread channels," in *Proc. 38th Asilomar Conference on Signals, Systems and Computers*, Nov. 2004, pp. 218–222.

[11] Y.-H. Chang, S.-H. Tsai, X. Yu, and C. C. J. Kuo, "Design and analysis of Channel-Phase-Precoded Ultra Wideband (CPPUWB) systems," in *Proc. IEEE Wireless Communications and Networking Conference*, Apr. 2006.

[12] S. Zhao and H. Liu, "Prerake diversity combining for pulsed UWB systems considering realistic channels with pulse overlapping and narrowband interference," in *Proc. IEEE GLOBECOM*, Nov. 2005, pp. 3784–3788.

[13] W. Cao, A. Nallanathan, and C. C. Chai, "On the multiple access performance of Prerake DS UWB System," in *Proc. of Milcom 2006*, Oct. 2006.

[14] J. R. Foerster, "Channel modeling sub-committee report final (doc: IEEE 802-15-02/490r1-sg3a)," Feb. 2002.

[15] T. Q. S. Quek and M. Z. Win, "Analysis of UWB transmitted-reference communication systems in dense multipath channels," *IEEE J. Select. Areas Commun.*, vol. 23, no. 9, pp. 1863–1874, Sept. 2005.

[16] K.-S. Song, "A globally convergent and consistent method for estimating the shape parameter of a generalized Gaussian distribution," *IEEE Trans. Inform. Theory*, vol. 52, no. 2, pp. 510–527, Feb. 2006.

[17] N. C. Beaulieu and S. Niranjayan, "New uwb receiver designs based on a gaussian-laplacian noise-plus-mai model," in *Proc. ICC 2007*, June 2007.

[18] K. Kokkinakis and A. K. Nandi, "Exponent parameter estimation for generalized gaussian probability density functions with application to speech modeling," *Signal Processing*, vol. 85, no. 9, pp. 1852–1858, Sept. 2005.

[19] E. A. Geraniotis and M. B. Pursley, "Error probability for direct-sequence spread-spectrum multiple-access communications–part II: approximations," *IEEE Trans. Commun.*, vol. COM-30, no. 5, May 1982.

[20] W. Cao, A. Nallanathan, B. Kannan, and C. C. Chai, "Exact BER analysis of DS-UWB multiple access system under imperfect power control," in *Proc. IEEE VTC 2005-Fall*, Sept. 2005, pp. 986–990.

Wei Cao (S'01) received her Bachelor and Master degrees from the Department of Electronics and Information Engineering, Huazhong University of Science and Technology (HUST), in 1999 and 2002, respectively. Since Aug 2003, she has been with the Department of Electrical and Computer Engineering, National University of Singapore (NUS) as a PhD candidate. Her research interests are in wireless communications, ultra-wideband communication systems, mobile communication systems and signal processing for communications.

Arumugam Nallanathan (S'97−M'00−SM'05) received the B.Sc. with honors from the University of Peradeniya, Sri-Lanka, in 1991, the CPGS from the Cambridge University, United Kingdom, in 1994 and the Ph.D. from the University of Hong Kong, Hong Kong, in 2000, all in Electrical Engineering. Since then, he has been an Assistant Professor in the Department of Electrical and Computer Engineering, National University of Singapore, Singapore. His research interests include OFDM systems, ultra-wide bandwidth (UWB) communication and localization, MIMO systems, and cooperative diversity techniques. In these areas, he has published over 100 journal and conference papers. He is a co-recipient of the Best Paper Award presented at 2007 IEEE International Conference on Ultra-Wideband.

He currently serves on the Editorial Board of IEEE TRANSACTIONS ON WIRELESS COMMUNICATIONS, IEEE TRANSACTIONS ON VEHICULAR TECHNOLOGY, John-Wiley's WIRELESS COMMUNICATIONS AND MOBILE COMPUTING and EURASIP JOURNAL OF WIRELESS COMMUNICATIONS AND NETWORKING as an Associate Editor. He served as a Guest Editor for EURASIP JOURNAL OF WIRELESS COMMUNICATIONS AND NETWORKING: Special issue on UWB Communication Systems–Technology and Applications. He also served as a technical program committee member for more than 25 IEEE international conferences. He currently serves as the General Track Chair for IEEE VTC'2008-Spring, Co-Chair for the IEEE GLOBECOM'2008 Signal Processing for Communications Symposium, and IEEE ICC'2009 Wireless Communications Symposium.

Chin Choy Chai received the Ph.D. and B. Eng. (Hons) Degrees, both in electrical engineering, from the National University of Singapore (NUS) in 1999 and 1995 respectively. He was a recipient of the NUS Research Scholarship from 1995 to 1998.

He has joined the Institute for Infocomm Research (formerly known as Centre for Wireless Communications, NUS and Institute for Communications Research) in 1998, where he is presently a Senior Research Fellow in their Modulation and Coding Department. His research interest is in digital modulation and detection, transmission rate and power control, performance enhancement of cellular spread spectrum systems, joint beamforming and power control for wireless relay channels.